ARL-RP-0528 ● AUG 2015

US Army Research Laboratory

Sample Size Induced Brittle-to-Ductile Transition of Single-Crystal Aluminum Nitride

by JJ Guo, KM Reddy, A Hirata, T Fujita, GA Gazonas, JW McCauley, and MW Chen

A reprint from Acta Materialia 88 (2015) 252–259

NOTICES

Disclaimers

The findings in this report are not to be construed as an official Department of the Army position unless so designated by other authorized documents.

Citation of manufacturer's or trade names does not constitute an official endorsement or approval of the use thereof.

Destroy this report when it is no longer needed. Do not return it to the originator.

ARL-RP-0528 ● AUG 2015

US Army Research Laboratory

Sample Size Induced Brittle-to-Ductile Transition of Single-Crystal Aluminum Nitride

by GA Gazonas and JW McCauley
Weapons and Materials Research Directorate, ARL

JJ Guo, KM Reddy, A Hirata, T Fujita, and MW Chen
WPI Advanced Institute for Materials Research, Tohoku University, Sendai 980-8577, Japan

A reprint from Acta Materialia 88 (2015) 252–259

REPORT DOCUMENTATION PAGE

Form Approved
OMB No. 0704-0188

1. REPORT DATE *(DD-MM-YYYY)*	2. REPORT TYPE	3. DATES COVERED (From - To)
Aug 2015	Reprint	January 2014–January 2015

4. TITLE AND SUBTITLE
Sample Size Induced Brittle-to-Ductile Transition of Single-Crystal Aluminum Nitride

5a. CONTRACT NUMBER

5b. GRANT NUMBER

5c. PROGRAM ELEMENT NUMBER

6. AUTHOR(S)
JJ Guo, K M Reddy, A Hirata, T Fujita, GA Gazonas, JW McCauley, and MW Chen

5d. PROJECT NUMBER

5e. TASK NUMBER

5f. WORK UNIT NUMBER

7. PERFORMING ORGANIZATION NAME(S) AND ADDRESS(ES)
US Army Research Laboratory
ATTN: RDRL-WMM-B
Aberdeen Proving Ground, MD 21005-5069

8. PERFORMING ORGANIZATION REPORT NUMBER
ARL-RP-0528

9. SPONSORING/MONITORING AGENCY NAME(S) AND ADDRESS(ES)

10. SPONSOR/MONITOR'S ACRONYM(S)

11. SPONSOR/MONITOR'S REPORT NUMBER(S)

12. DISTRIBUTION/AVAILABILITY STATEMENT
Approved for public release; distribution unlimited.

13. SUPPLEMENTARY NOTES
A reprint from Acta Materialia 88 (2015) 252–259

14. ABSTRACT

Ceramics are known to be mechanically hard, chemically inert and electrically insulating for many important applications. However, they usually suffer from brittleness and have moderate strength that strongly depends on their microscopic structure. In this study, we report a size induced brittle-to-ductile transition in single-crystal aluminum nitride (AlN). When the specimen diameters are smaller than ~3–4 μm, AlN micropillars show metal-like plastic flow under room-temperature uniaxial compression. The unprecedented plastic strain of ~5–10% together with the ultrahigh strength of ~6.7 GPa has never been achieved before. Transmission electron microscopy demonstrates that dislocations play a dominant role in the plasticity of the micro-sized AlN.

15. SUBJECT TERMS
aluminum nitride, ceramic, dislocations, TEM, Raman spectroscopy, micropillar

16. SECURITY CLASSIFICATION OF:			17. LIMITATION OF ABSTRACT	18. NUMBER OF PAGES	19a. NAME OF RESPONSIBLE PERSON
a. REPORT	b. ABSTRACT	c. THIS PAGE			GA Gazonas
Unclassified	Unclassified	Unclassified	UU	14	19b. TELEPHONE NUMBER (Include area code) (410) 306-0863

Available online at www.sciencedirect.com

ScienceDirect

Acta Materialia 88 (2015) 252–259

Acta MATERIALIA

www.elsevier.com/locate/actamat

Sample size induced brittle-to-ductile transition of single-crystal aluminum nitride

J.J. Guo,[a,1] K. Madhav Reddy,[a,1] A. Hirata,[a] T. Fujita,[a] G.A. Gazonas,[b] J.W. McCauley[b] and M.W. Chen[a,*]

[a] *WPI Advanced Institute for Materials Research, Tohoku University, Sendai 980-8577, Japan*
[b] *U.S. Army Research Laboratory, Aberdeen Proving Ground, MD 21005, USA*

Received 9 August 2014; revised 13 January 2015; accepted 16 January 2015

Abstract—Ceramics are known to be mechanically hard, chemically inert and electrically insulating for many important applications. However, they usually suffer from brittleness and have moderate strength that strongly depends on their microscopic structure. In this study, we report a size induced brittle-to-ductile transition in single-crystal aluminum nitride (AlN). When the specimen diameters are smaller than ~3–4 μm, AlN micropillars show metal-like plastic flow under room-temperature uniaxial compression. The unprecedented plastic strain of ~5–10% together with the ultrahigh strength of ~6.7 GPa has never been achieved before. Transmission electron microscopy demonstrates that dislocations play a dominant role in the plasticity of the micro-sized AlN.

Keywords: Ceramics; Micropillar; Plastic deformation; Size effect; Transmission electron microscopy

1. Introduction

Covalently bonded ceramics exhibit many distinctive physical and mechanical properties, compared to metallic and polymeric materials, but the propensity toward brittle fracture has limited their applications especially in forming and load bearing operations [1–6]. As exceptions, only a handful of ceramics show room-temperature plasticity via anomalous deformation processes, such as martensitic transformation [1,2], kink bands [3] and grain boundary sliding [4,7], or subjected to extreme loading conditions, such as shock [6,8], high pressure [9–11] and strain confinement [11–13]. Nevertheless, large dislocation plasticity is rarely seen in high strength ceramics during room-temperature uniaxial deformation [14].

Aluminum nitride (AlN) is a high-performance covalently bonded ceramic material and possesses high hardness and strength with relatively low specific density. It has a stable wurtzite-type structure with a smaller c_0/a_0 ratio of ~1.60 than the formal hexagonal close-packed lattice (1.633) [11]. AlN has been widely used in electronics and as a structural ceramic material. In the past decades, particular attention has been paid to its mechanical stability. Wilkins et al. first pointed out the importance of inelastic deformation in the impact performance of AlN [15]. Moreover, it has been reported that hydrostatic confinement facilitates dislocation plasticity of AlN [11,13]. However, the room temperature plasticity cannot be retained in confinement-free AlN, which always fails in a brittle manner without any plastic strain under quasi-static uniaxial deformation [11,15–18].

Since the advent and development of microsystems and nanotechnology, the understanding of micro-scale deformation and failure mechanisms of advanced materials has been gaining importance. It was recently observed that the deformation mechanisms of metallic alloys have shown a consistent difference in strength and plasticity between micro-sized and bulk specimens [19–21]. These findings strongly suggest that specimen size may influence the activation and motion of dislocations, and hence the mechanical response of ductile metals. Compared to metallic materials, the mechanical response of ceramics is expected to be strongly size-dependent because of their rigid ionic and covalent bonding which is highly sensitive to defects and flaws. However, for strong and relatively brittle ceramics, the size dependence of their strength and ductility has not been well explored [4,22–24]. Recently, the size induced plasticity has been observed in covalent and ionic crystals, such as sapphire [25], GaAs [26], SiC [27] and MgO [28], during room-temperature microcompression. These studies indicate that decreasing sample sizes to the order of micrometer scale can suppress cracking and leads to the change in the deformation behavior from brittle to ductile [29,30]. In this work, we report the deformation behavior

* Corresponding author; e-mail: mwchen@wpi-aimr.tohoku.ac.jp
[1] These authors contributed equally to this work.

http://dx.doi.org/10.1016/j.actamat.2015.01.043
1359-6462/

of single crystal AlN micropillars subjected to uniaxial compression along the [0001] and [10$\bar{1}$0] axes. The microcompression experiments at a small length scale reveal unprecedented large dislocation plasticity in AlN that has been conventionally characterized as a brittle ceramic.

2. Experimental details

2.1. Materials and microcompression testing

AlN single crystals used in this study were commercially obtained from Fairfield Crystal Technology. The single crystals appear in the form of a hexagonal pillar as shown in the inset of Fig. 1. Micropillars for compression testing have the top surfaces parallel to the basal plane (0001) and side plane (10$\bar{1}$0), respectively. The microcompression technique developed by Uchic et al. [20] has proven itself as a reliable way to explore the mechanical behavior of micro-size specimens. Here we have used a focus ion beam (FIB) system to fabricate columnar micropillars with diameters ranging from ~2.5 to 20 μm and the aspect ratio approximately 2.5:1 for diameters below 10 μm and 2:1 for above 10 μm samples. The micropillars located in the center of large trenches which can guarantee that a flat punch is in contact only with the pillars during compression testing. The uniaxial compression tests were carried out by nanoindentation device (Shimadzu W201S) and the tests were performed using flat punch indenters with diameters of 10 μm and 40 μm, respectively. All the single-crystal micropillars were compressed to a preset depth of 10% to 15% of the initial heights of the pillars at a strain rate of $\sim 10^{-4}$ 1/s. The engineering stress–strain curves were calculated based on instantaneous measurements of load–displacement data and the specimen dimensions were determined precisely by scanning electron microscopy (SEM) after FIB fabrication. All the tests were conducted at room temperature. The active slip systems were determined on the basis of crystallographic and geometric analyses with the help of Schmid's law.

2.2. Microstructure characterization

The single crystal nature of the AlN specimens was verified by X-ray diffraction (XRD, RINT 2200, Rigaku X-ray diffractometer) and Raman Microscopy (Renishaw, U.K.). The cross-sectional TEM specimens of compressed micropillars were prepared by a lift-out FIB technique using a dual-beam FIB/SEM system (JEOL, JIB-4600F). The deformation regions of micropillars were characterized by TEM (JEOL JEM-2100F) operated at 200 kV.

3. Results

3.1. Orientation determination of single-crystal AlN

The single-crystal nature of the AlN specimens used in this study was determined by Raman spectroscopy. Raman spectra taken from polished basal plane (0001) and prismatic plane (10$\bar{1}$0) present an obvious crystallographic orientation dependence of Raman scattering as shown in Fig. 1. Along the direction perpendicular to the (0001) plane, only the E_2^1, E_2^2 and A_1(LO) phonons, centered at

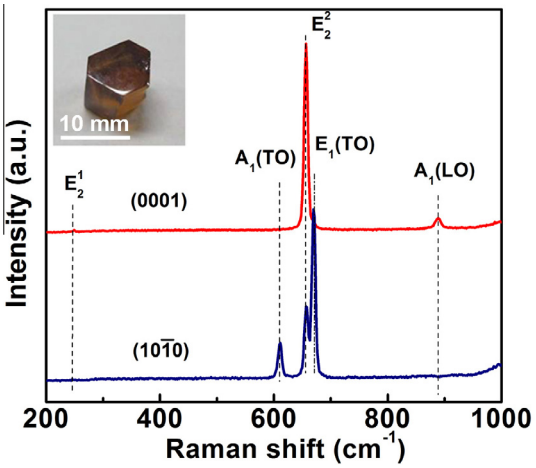

Fig. 1. Raman spectroscopy of single-crystal AlN. Raman spectra were taken from the basal plane (0001) and prismatic plane (10$\bar{1}$0) of single crystal AlN. Inset photograph shows an as-received AlN single crystal.

249.1, 656.4, and 888.2 cm^{-1}, respectively, are observed in the backscattering Raman spectrum. In the direction perpendicular to the (10$\bar{1}$0) plane, the TO component of A_1(TO) at 611.3 cm^{-1} and E_1(TO) at 669.8 cm^{-1} are detected while the A_1(LO) becomes inactive. These stress free phonon modes of (0001) and (10$\bar{1}$0) planes are fully consistent with the selection rules for the backscattering geometry of single-crystal AlN [31,32]. Separate X-ray diffraction further confirms the single-crystal nature and crystallographic orientations of the samples (data not shown here). Both diffraction spectra from basal and prismatic planes show a single-crystal feature and the diffraction peaks are fully consistent with the prediction from the theoretical structure model of wurtzite AlN.

3.2. AlN micropillar compression along [0001] direction

A representative engineering stress–strain curve of a (0001) micropillar with a diameter of 4 μm is shown in Fig. 2a. The compressive deformation response is characterized by linear elastic behavior up to ~6 GPa where macroscopic yielding initiates, followed by ~7% plastic flow and 6.7 GPa ultimate strength before failure. One important aspect of the stress–strain curve is the work hardening behavior, which is frequently observed in ductile metals but rarely in ceramics. Since work hardening usually originates from the interaction of dislocations from different slip systems, it indicates that multiple slip systems are activated in the (0001) single crystal. Fig. 2b and c shows the SEM images of the (0001) micropillar before and after uniaxial compression. Corresponding to the large plastic strain, the SEM micrograph reveals the presence of multiple shearing traces along two intersecting slip planes on the pillar surface (Fig. 2c). These observations indicate that at least two independent slip systems are activated during the plastic deformation. The slip planes have an angle of ~55° with respect to the (0001) plane and could correspond to either {2$\bar{1}\bar{1}$2} or {1$\bar{1}$01} planes. The slip directions for each of these planes are <11$\bar{2}$3> ($c + a$ type). Both of the slip systems have been frequently observed in the wurtzite structure [33], which are expected to provide five independent slip modes to satisfy von Mises criterion for continuous

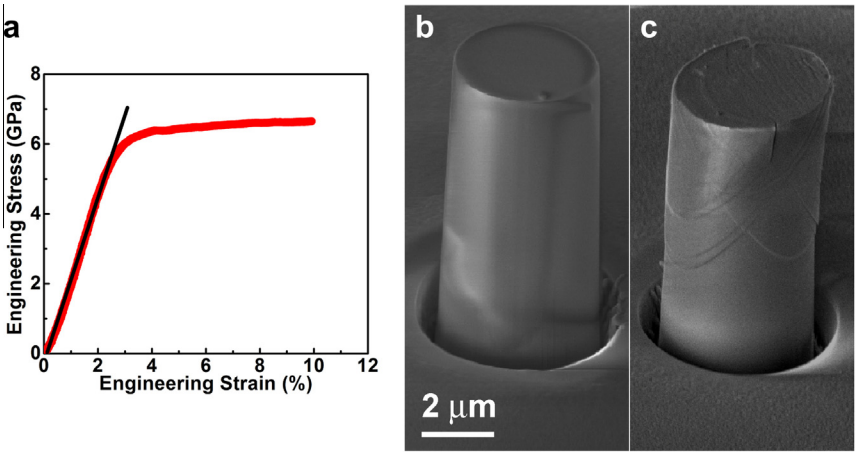

Fig. 2. Mechanical behavior of single-crystal (0001) AlN micropillars. (a) Engineering stress–strain curve of a 4 μm single-crystal AlN micropillar compressed along the [0001]direction. (b) SEM image of the as-fabricated 4 μm diameter micropillar. (c) The morphology of the plastically deformed micropillar with~7% plastic strain and ~6.7 GPa ultimate strength.

plastic deformation. In comparison with the $\{1\bar{1}01\}<11\bar{2}3>$ slip system, the $<11\bar{2}3>\{2\bar{1}\bar{1}2\}$ slip system is readily activated due to its large Schmid factor (~0.45) and the largest net driving force when loading along <0001> direction [34,35]. To further investigate the micro-mechanisms of the plastic deformation, a deformed micropillar was sliced into a thin foil along the <0001> direction using a FIB system for transmission electron microscopy (TEM) characterization [36]. Fig. 4a and b show the cross-sectional TEM image and diffraction pattern oriented along the <0001> direction. The sliced TEM specimen is only one-sided cross section of the basal plane and the selection of sliced plane is shown with dotted lines in Fig 3a. Fig. 4c and d show the bright-field and weak-beam TEM images of the deformed pillar. The slip bands consist of a high density of dislocations that are appropriately parallel to each other. Consistent with the slip traces on the micro-pillar surface, only one major slip system can be imaged from this orientation while the two intersecting dislocation slip systems shown in Fig. 3a cannot be seen in the thin TEM foil. On the basis of the selected area electron diffraction, the slip plane can be indexed as $\{2\bar{1}\bar{1}2\}$. The reflecting vector for the weak-beam image is [0002] and hence the dislocations have non-basal vectors. Thus, the Burges vector of the dislocations should be $1/3<11\bar{2}3>$, which is consistent with the SEM slip trace analysis and the prediction derived from Schmid factor calculations [35]. In this loading configuration, dislocation slip along six different planes is equally favorable. Therefore, the work hardening in the single-crystal AlN micro-pillars is essentially identical to that in ductile metals and originates from the interaction of dislocations on intersecting slip systems. In addition, a number of dislocations from the basal slip system have also been observed, which may be aroused from the small misalignment in the microcompression testing. Interestingly, the dislocation plasticity of the single-crystal AlN strongly depends on specimen sizes. As shown in Fig. 5a and b, the large plastic strain can only be obtained from small specimens with diameters of ~2.5 and 4 μm. Further increasing the sample diameter to ~5.8 μm leads to the dramatic loss in plasticity. When the sample diameters are larger than 10 μm, the samples fail in a brittle manner by shattering without any plastic strain (Fig. 5c and d), showing the typical mechanical behavior of brittle ceramics.

3.3. AlN micropillar compression along $[10\bar{1}0]$ direction

The dislocation plasticity can also be achieved from the prismatic deformation of $(10\bar{1}0)$ micropillars. Fig. 6a illustrates an engineering stress–strain curve of a $(10\bar{1}0)$ micropillar with the diameter of ~3 μm. After initially yielding at ~1.5 GPa, the flow strength of the specimen gradually increases to 2.25 GPa with the accumulated plastic strain up to ~10%. The significant difference in the ultimate strength between basal and prismatic compression of AlN arises mainly from the variation of the activated dislocation slip systems [37,38]. Fig. 6b and c depicts the SEM images of the $(10\bar{1}0)$ micropillar before and after deformation. One primary slip band can be observed on the surface of the deformed pillar. The angle between this slip plane and the loading direction of $[10\bar{1}0]$ is approximately 60°, close to the $(1\bar{1}00)$ plane. Bright- and dark-field TEM observations (Fig. 6d and e) confirm the slip plane is $(1\bar{1}00)$. Since no Burgers vector with a component parallel to the *c* axis was identified, the slip system can be deduced to be $<11\bar{2}0>(1\bar{1}00)$, corresponding to the primary slip trace in Fig. 6c. The plastic deformation along the prismatic direction also shows the specimen size dependence. Although the stress–strain curves do not present obvious difference in plastic strains (Fig. 7a), SEM micrographs of the deformed micropillars demonstrate that the small specimens with a diameter of ~2–5 μm plastically deform by dislocations along the $<1\bar{1}00>(1\bar{1}00)$ slip system, whereas the specimens with a diameter larger than 10 μm actually fail by top surface splitting along the (0001) basal plane at the very early stage of deformation (Fig. 7b and c). Since the (0001) basal plane is parallel to the loading direction of $[10\bar{1}0]$, the top surface cracked pillars can continuously deform but give rise to bumpy stress–strain curves. This type of specimen failure has been observed in magnesium oxide and gallium arsenide micropillars [24,30,39] and is also a common failure mode in unconfined uniaxial compression of rocks.

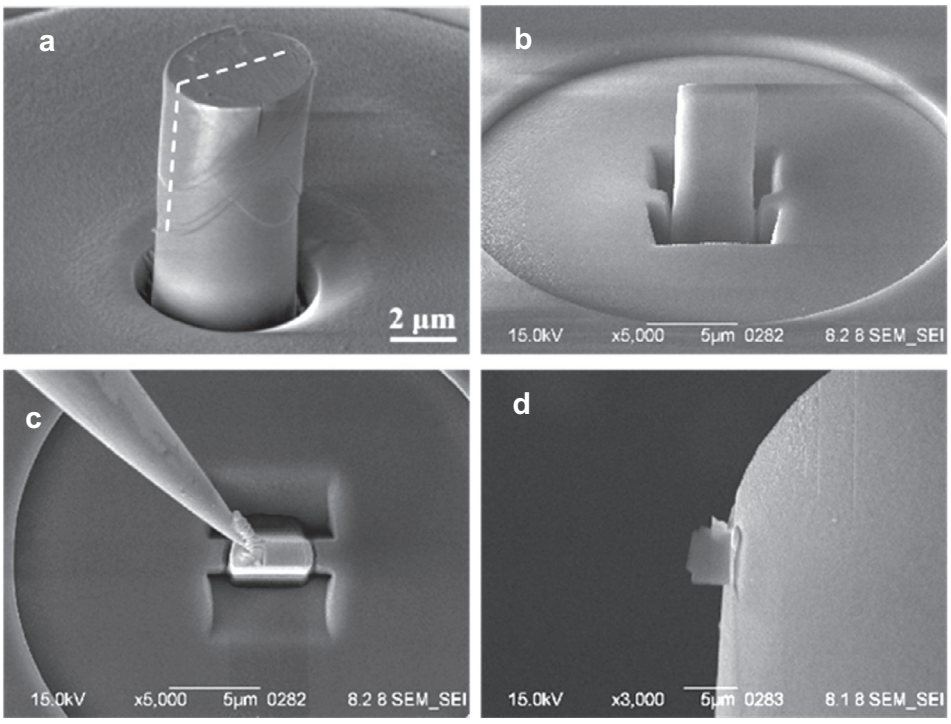

Fig. 3. Fabrication procedure of a cross-sectional TEM specimen of a compressed micropillar. (a) SEM image of a deformed (0001) micropillar. The dash line indicates the orientation of the TEM foil, which is vertical to the selected slipping planes. (b) TEM foil fabricated by removing the surrounding matrix. (c) Transferring the wedge-sharp specimen to a copper grid by a FIB micro-probe. (d) Side view of the sliced specimen after a final milling. The TEM foil is welded on the Cu grid using tungsten deposition.

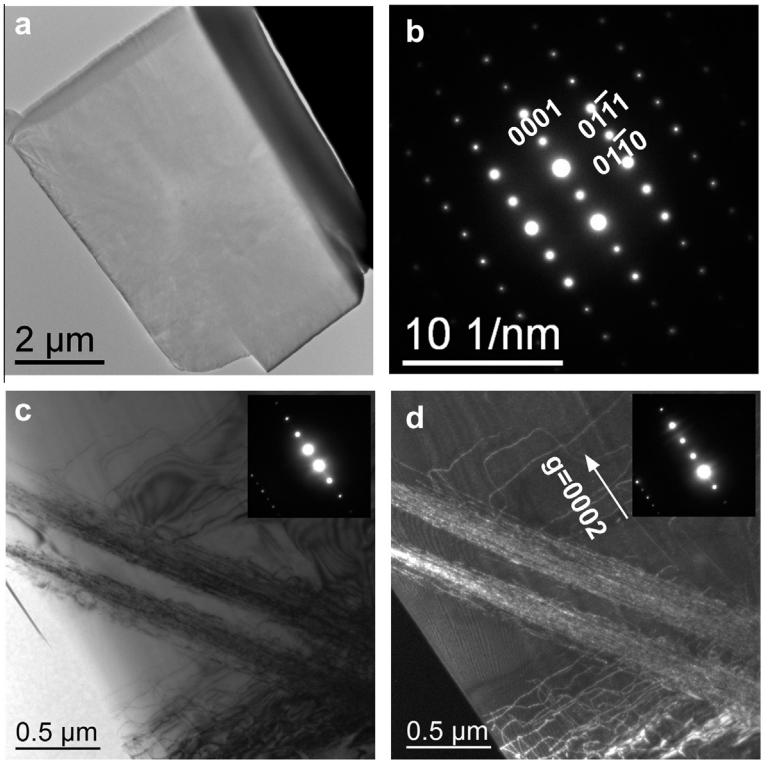

Fig. 4. TEM micrograph of a deformed (0001) micropillar. (a) Low-magnification cross-sectioned TEM image. (b) Corresponding selected area electron diffraction pattern showing the orientation of the TEM specimen; and (c) Bright-field TEM image showing the dislocations in two parallel slip bands in the deformed micropillar. The micrograph was imaged under a two-beam condition with the diffraction vector (g) parallel to [0002]. (d) $g/3g$ weak beam TEM image showing a high density of dislocations in slip bands.

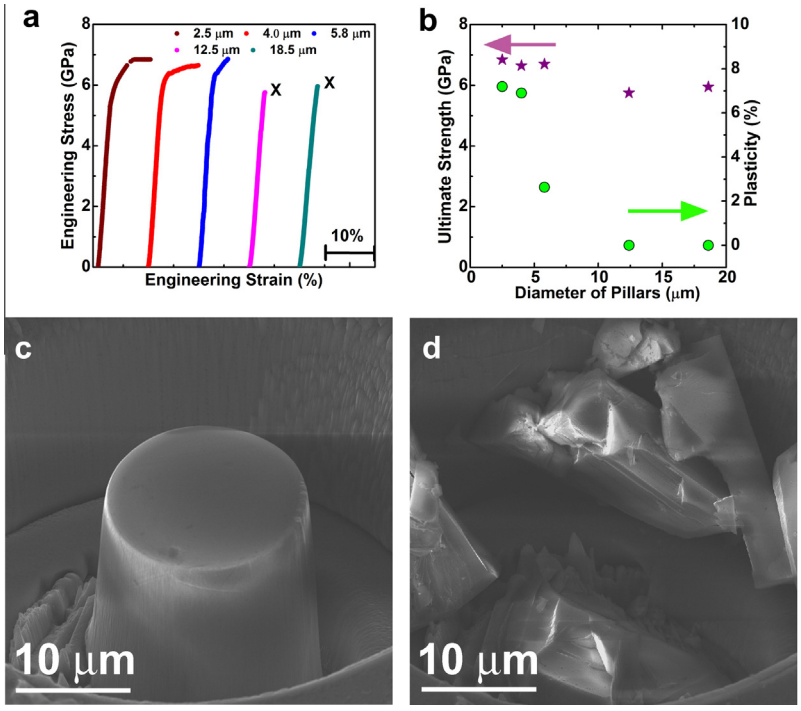

Fig. 5. Size dependence of mechanical properties of (0001) AlN single crystals. (a) Representative engineering stress–strain curves of micropillars with diameters ranging from ~2.5 to 20 μm. The constant loading rate is 13.2 mN/s (strain rate $\sim 10^{-4}$/s). All these microsize specimens were deformed to a preset depth of 10–15% of their respective height and fractured micropillars are shown by cross mark (×). (b) The measured ultimate (failure) strength and plasticity *vs.* the diameters of micropillars. (c) Typically SEM image of an as-fabricated micropillar with a diameter of 18.5 μm; and (d) the failed specimen in a brittle manner prior to plastic yielding.

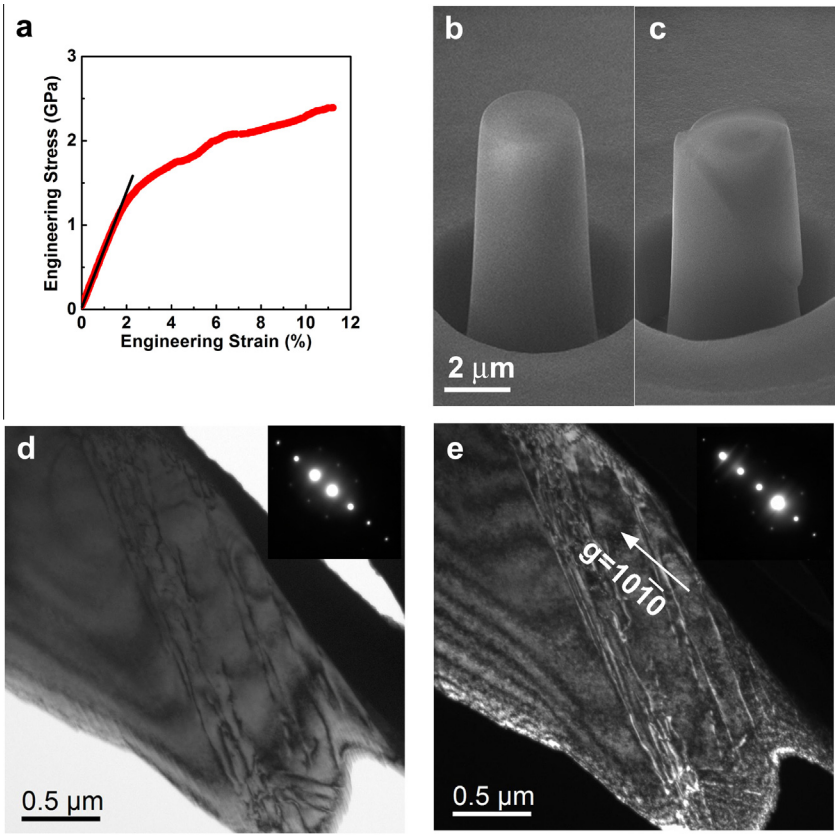

Fig. 6. Mechanical behavior of a (10$\bar{1}$0) AlN single crystal. (a) Depicted engineering stress–strain curve of a single-crystal AlN micropillar compressed along [10$\bar{1}$0] prism direction. (b) SEM image of the as-fabricated micropillar with a diameter of 3 μm; and (c) Plastically deformed specimen with a visible slip band. (d) Bright-field TEM image of the deformed micro-pillar showing a high density of dislocations within a slid band. (e) Weak-beam TEM micrograph of dislocations in the *g*/3*g* imaging condition.

4. Discussion

Fig. 8a shows the comparison of the maximum plastic strain and ultimate strength of AlN with other high-strength single crystals and amorphous alloys tested by micro-compression with pillar diameters ranging from ~500 nm to 5 μm [22,25,27–29,40–44]. The general trend from these data, regardless of deformation mechanisms, is that the higher strength of materials typically accompany with lower plasticity. Nevertheless, different from other ultra-high strength materials, the single-crystal AlN, especially (0 0 0 1) single crystals, shows an extraordinary combination of high strength and plasticity. Fig 8b summarizes the sample size effect on normalized strength of single crystals at a small length scale [22,25,27–29,40–42], in which the shear strength (τ) is normalized by the shear modulus (G) and fitted by a power law equation of sample diameters (d):

$$\frac{\tau}{G} = Bd^{-n}. \quad (1)$$

As shown in the plots, normalized shear strength remains to be one of the highest among strong and brittle materials and has smaller scaling factor (n) in comparison with the less hard bcc and fcc single-crystal metals. The scaling factors (n) of AlN (0 0 0 1) and AlN (1 0 $\bar{1}$ 0) are 0.035 and 0.08, respectively, about one order of magnitude smaller than that of bcc (0.25) and fcc (0.6) metals [29,41]. The small exponent n indicates that the strength of AlN is less sensitive to the sample sizes although there is significant size dependence in plasticity in the same length scale. The decoupling between the strength and plasticity implies that the obvious size effect in plasticity of AlN, but not strength, may not originate from the flaw controlled Weibull distribution which is often observed in brittle materials.

Dislocation behavior is the primary micromechanism for the plastic deformation of ductile metals while the mechanical performance of high-strength ceramics is often dominated by brittle fracture at room temperature. Recent microcompression experiments show that brittle ceramics could be plastically deformed by dislocations at small length scale [25,27,30]. For AlN, both single-crystal and polycrystalline samples at a macroscopic length scale always fails in a brittle manner at room temperature prior to plastic yielding although hydrostatic stress state introduced by mechanical confinements can significantly suppress the brittle failure and gives rise to dislocation plasticity [11–13]. Different from previous observations, in this study we found that brittle AlN can plastically flow like metals with considerable dislocation plasticity when specimen sizes are smaller than a critical value of ~4 μm, presenting a remarkable size-induced brittle-to-ductile transition in this high-strength covalently-bonded ceramic.

In general, the significant size dependence of strength and plasticity follows the Weibull distribution, i.e., larger specimens behave in a more brittle fashion due to the higher probability of having a critically oriented flaw in the larger volume. However, the abrupt change in plasticity around the critical sample diameter, together with insignificant strength difference, cannot be described by Weibull-like behavior (Fig. 5b). The weak dependence of the normalized

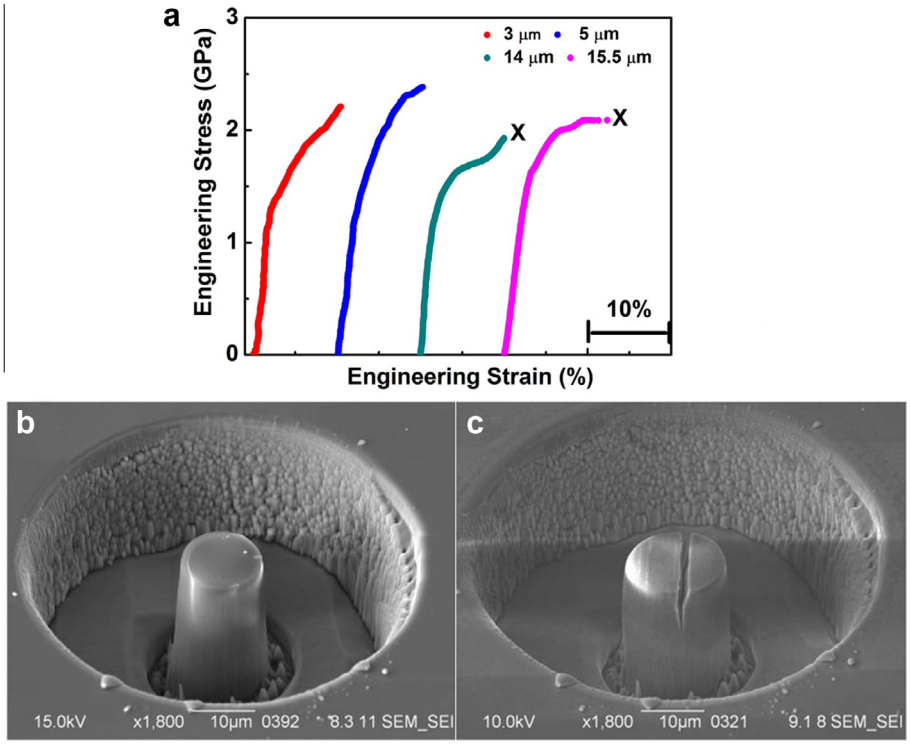

Fig. 7. Mechanical behavior of single-crystal AlN micropillars compressed along a [1 0 $\bar{1}$ 0] direction. (a) Representative stress–strain curves of micropillars with diameters ranging from 3 to ~16 μm and heights of 5–30 μm. The compression tests were conducted at a constant loading rate of 13.2 mN/s (strain rate ~10^{-4} 1/s). All micropillars were deformed to a preset displacement of 10–15% of their respective height. The curves marked by cross (×) indicates the specimen failure by top surface splitting. (b) SEM image of an as-fabricated 14 μm diameter micropillar. (c) SEM image of the tested 14 μm diameter micropillar. Note the specimens with a diameter larger than 10 μm actually fail by top surface splitting along the (0 0 0 1) basal plane at very early stage of deformation.

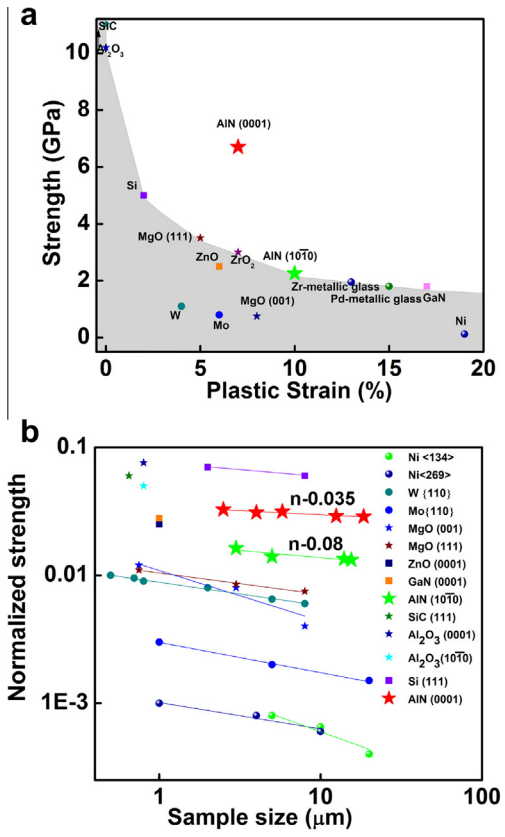

Fig. 8. Comparison of micropillars plastic strain and strength of single-crystal (0001) and (10$\bar{1}$0) AlN with other high strength materials. (a) Representative strength *vs.* plastic strain before fracture of other high strength single crystals and amorphous alloys were measured by micropillars with diameters between ~500 nm and 5 μm [22,25,27–29,40–44]. Different from other ultra-high strength materials, AlN, especially (0001) single crystals, has both extraordinary strength and plasticity. (b) Normalized shear strength *vs.* Sample size is shown for different classes of single crystals [22,25,27–29,40–42]. A scaling exponent of AlN (0001) and (10$\bar{1}$0) is approximately 0.035 and 0.08.

strength on sample diameter suggests that the critical shear strength required to activate dislocations does not change with sample size. Therefore, the size effect in plasticity may originate from an intrinsic transition in material deformation behavior and the competition between dislocation nucleation/motion and crack formation/propagation. Since the sample size variation from 4 to 10 μm should not obviously change the critical shear stress for dislocation activation, the significant size effect appears to be dominated by the crack formation and propagation. In fact, the critical specimen size observed in this study is very close to the value (several micrometers) of ceramic transition flaw size $\alpha = \psi(K_{IC}/\sigma_y)^2$, which is determined by the fracture toughness (K_{IC}), yield strength (σ_y) and flaw geometry constant (ψ) [45]. When the specimen diameters are smaller than the transition flaw size, the small specimens cannot provide sufficient elastic energy for rapid crack propagation and specimen failure occurs by plastic deformation. Based on the K_{IC} value (~3.925 MPa $m^{1/2}$) of AlN and the yield strength measured by this study, the critical sample size for the brittle-to-ductile transition is ~2–4 μm, fairly consistent with the experimental observation.

It has been suggested that the stress intensity factor of cracks decreases with the sample size of high strength materials. Below a critical sample diameter, the stress intensity factor is always less than the fracture toughness of the materials and, therefore, the cracking no longer occurred [26,29–30]. We calculated the stress intensity factor of AlN at a small sample diameter on the basis of the model proposed by Howie et al. [23] and found that at a diameter smaller than 4 μm micropillars do not initiate a crack because the fracture toughness (3.925 MP $am^{1/2}$) is larger than the stress intensity factor (2.3 MP $am^{1/2}$) that is required for crack nucleation.

Regardless of the underlying micromechanistic causes of the size-induced brittle-to-ductile transition observed in the single-crystal AlN, the finding that the single crystal AlN micropillars exhibit an extraordinary combination of the ultrahigh strength(~6.7 GPa) with high plasticity (5–10%) (Fig. 8), in comparison with the reported microcompressive properties of other high-strength materials [22,25,27–29,40–44], has important implications for developing high-performance ceramic materials with both high strength and good ductility. The new strategy of manipulating the structure and size of materials conventionally classified as being strong but brittle into strong and ductile could have important applications in MEMS and other emerging small-scale nano-device applications.

5. Conclusions

In this work we systematical studied the microcompressive properties of single crystal AlN at room temperature. It was found that there is a size induced brittle-to-ductile transition in the brittle but strong material. SEM and TEM characterizations reveal that the transition is associated with the activation of dislocation plasticity. The main results are summarized as follows:

(1) The engineering stress–strain curves of [0001] AlN with a diameter smaller than 4 μm shows ultrahigh strength of ~6.7 GPa with unprecedented plastic strain over ~7%, while the samples with a larger size fail in a brittle manner prior to plastic yielding. The postmortem SEM observations of plastically deformed smaller pillars reveal intersection of multiple slip bands, indicating that at least two independent slip systems are activated in the plastic deformation.

(2) The size induced brittle-to-ductile transition can also be observed from [10$\bar{1}$0] micropillars. The samples with a diameter smaller than 4 μm show a large plastic strain up to ~10% while the ultimate strength is ~2.25 GPa, much lower than that of the [0001] pillars. Therefore, the strength of the single-crystal AlN is mainly determined by the crystal orientation whereas the plasticity is controlled by sample sizes.

(3) Both [0001] and [10$\bar{1}$0] pillars with sizes larger than the critical value fail by cracking (cleavage for [0001] crystals and top surface splitting for [10$\bar{1}$0] samples) in the early stage of compression testing. Thus, the size induced brittle-to-ductile transition arises from the competition between the dislocation behavior and crack initiation/propagation.

(4) Since the sample size variation around the critical value of ~4 μm should not obviously change the critical shear stress for dislocation nucleation and motion, the significant sample size effect observed in this study appears to be dominated by the crack formation and propagation., which is supported by the consistence between the critical sample size for the brittle-to-ductile transition and the value of ceramic transition flaw size.

(5) TEM and SEM characterization demonstrates that the large plastic strains achieved from small samples are accomplished by dislocation plasticity and the activated dislocation slip systems are in agreement with the calculations of Schmid factors based on the loading conditions and crystal geometry.

(6) The brittle-to-ductile transition at a small length scale has important applications in manipulating the structure and size of materials conventionally classified as being strong but brittle into strong and ductile for MEMS and other emerging small-scale nano-device applications.

Acknowledgements

This work was supported by "World Premier International (WPI) Center Initiative for Atoms, Molecules and Materials", MEXT, Japan; U.S. Army International Technology Center Pacific (ITC-PAC) of Tokyo; and U. S. Army Research Lab through Johns Hopkins University.

References

[1] R.C. Garvie, R.H. Hannink, R.T. Pascoe, Nature 258 (1975) 703.
[2] R.M. McMeeking, A.G. Evans, J. Am. Ceram. Soc. 65 (1982) 242.
[3] M.W. Barsoum, T. Zhen, S.R. Kalidindi, M. Radovic, A. Murugaiah, Nat. Mater. 2 (2003) 107.
[4] K. Madhav Reddy, J.J. Guo, Y. Shinoda, T. Fujita, A. Hirata, J.P. Singh, J.W. McCauley, M.W. Chen, Nat. Commun. 3 (2012) 1052.
[5] M.W. Chen, J.W. McCauley, D.P. Dandekar, N.K. Bourne, Nat. Mater. 5 (2006) 614.
[6] M.W. Chen, J.W. McCauley, K.J. Hemker, Science 299 (2003) 1563.
[7] H. Muto, Y. Takahashi, T. Futami, M. Sakai, J. Euro. Ceram. Soc. 22 (2002) 2437.
[8] E.K. Beauchamp, M.J. Carr, R.A. Graham, J. Am. Ceram. Soc. 68 (1985) 696.
[9] X.Q. Yan, Z. Tang, L. Zhang, J.J. Guo, C.Q. Jin, Y. Zhang, T. Goto, J.W. McCauley, M.W. Chen, Phys. Rev. Lett. 102 (2009).
[10] K. Edalati, S. Toh, Y. Ikoma, Z. Horita, Scripta Mater. 65 (2011) 974.
[11] H.C. Heard, C.F. Cline, J. Mater. Sci. 15 (1980) 1889.
[12] G. Ravichandran, G. Subhash, J. Am. Ceram. Soc. 77 (1994) 263.
[13] G. Hu, K.T. Ramesh, B. Cao, J.W. McCauley, J. Mech. Phys. Solids 59 (2011) 1076.
[14] Y. Zou, R. Spolenak, Phil. Mag. Lett. 93 (2013) 431.
[15] Wilkins MLC, C. F, Honodel, C. A. Lawrence Livermore Laboratory 1969: Rep. UCRL.
[16] J. Lankford, W.W. Predebon, J.M. Staehler, G. Subhash, B.J. Pletka, C.E. Anderson, Mech. Mater. 29 (1998) 205.
[17] I. Yonenaga, J. Phys. Cond. Matter 14 (2002) 12947.
[18] P.S. Branicio, R.K. Kalia, A. Nakano, P. Vashishta, Phys. Rev. Lett. 96 (2006) 065502.
[19] F.F. Csikor, C. Motz, D. Weygand, M. Zaiser, S. Zapperi, Science 318 (2007) 251.
[20] M.D. Uchic, D.M. Dimiduk, J.N. Florando, W.D. Nix, Science 305 (2004) 986.
[21] Q. Yu, Z.-W. Shan, J. Li, X. Huang, L. Xiao, J. Sun, E. Ma, Nature 463 (2010) 335.
[22] A. Lai, Z. Du, C.L. Gan, C.A. Schuh, Science 341 (2013) 1505.
[23] P.R. Howie, S. Korte, W.J. Clegg, J. Mater. Res. 27 (2012) 141.
[24] D. Jang, L.R. Meza, F. Greer, J.R. Greer, Nat. Mater. 12 (2013) 893.
[25] A. Montagne, S. Pathak, X. Maeder, J. Michler, Ceram. Int. 40 (2014) 2083.
[26] F. Östlund, P.R. Howie, R. Ghisleni, S. Korte, K. Leifer, W.J. Clegg, J. Michler, Philos. Mag. 91 (2010) 1190.
[27] C. Shin, H.-H. Jin, W.-J. Kim, J.-Y. Park, J. Am. Ceram. Soc. 95 (2012) 2944.
[28] S. Korte, J.S. Barnard, R.J. Stearn, W.J. Clegg, Int. J. Plast. 27 (2011) 1853.
[29] S. Korte, W.J. Clegg, Philos. Mag. 91 (2010) 1150.
[30] F. Östlund, K. Rzepiejewska-Malyska, K. Leifer, L.M. Hale, Y. Tang, R. Ballarini, W.W. Gerberich, J. Michler, Adv. Funct. Mater. 19 (2009) 2439.
[31] P. Pandit, D.Y. Song, M. Holtz, J. Appl. Phys. 102 (2007) 113510.
[32] M. Kuball, J.M. Hayes, A.D. Prins, N.W.A. van Uden, D.J. Dunstan, Y. Shi, J.H. Edgar, Appl. Phys. Lett. 78 (2001) 724.
[33] M.H. Yoo, Metall. Trans. A 12 (1981) 409.
[34] S. Srinivasan, L. Geng, A. Ponce, Y. Narukawa, S. Tanaka, Phys. status solidi 7 (2003) 2440.
[35] P. Pant, J.D. Budai, J. Naryan, Acta Mater. 58 (2010) 1097.
[36] S. Kuwano, T. Fujita, D. Pan, K. Wang, M.W. Chen, Mater. Trans. 49 (2008) 2091.
[37] Hull D. second ed., Pergamon Press, Oxford 1975.
[38] V. Audurier, J.L. Demenet, J. Rabier, Philos. Mag. A 77 (1998) 843.
[39] J. Michler, K. Wasmer, S. Meier, F. Östlund, K. Leifer, Appl. Phys. Lett. 90 (2007).
[40] J.R. Greer, J.T.M. De Hosson, Prog. Mater. Sci. 56 (2011) 654.
[41] M.D. Uchic, P.A. Shade, D.M. Dimiduk, Annu. Rev. Mater. Res. 39 (2009) 361.
[42] Q. Sun, Q. Guo, X. Yao, L. Xiao, J.R. Greer, J. Sun, Scripta Mater. 65 (2011) 473.
[43] B.E. Schuster, Q. Wei, T.C. Hufnagel, K.T. Ramesh, Acta Mater. 56 (2008) 5091.
[44] J.-Y. Kim, D. Jang, J.R. Greer, Acta Mater. 58 (2010) 2355.
[45] B.R. Lawn, J. Mater. Res. 19 (2004) 22.

1 (PDF) DEFENSE TECHNICAL INFORMATION CTR DTIC OCA

2 (PDF) DIRECTOR US ARMY RESEARCH LAB RDRL CIO LL IMAL HRA MAIL & RECORDS MGMT

1 (PDF) GOVT PRINTG OFC A MALHOTRA

49 (PDF) DIR USARL
RDRL CIH C
J KNAP
RDRL WM
B FORCH
S KARNA
J MCCAULEY
RDRL WML B
I BATYREV
E BYRD
S IZVYEKOV
B RICE
D TAYLOR
N WEINGARTEN
RDRL WML H
C MEYER
B SCHUSTER
RDRL WMM
J BEATTY
R DOWDING
J ZABINSKI
RDRL WMM B
C FOUNTZOULAS
G GAZONAS
D HOPKINS
B LOVE
B POWERS
R WILDMAN
C YEN
J YU
RDRL WMM D
S WALSH
RDRL WMM E
J LASALVIA
P PATEL
J SINGH
J SWAB
RDRL WMM F
T SANO
M TSCHOPP
RDRL WML G
J ANDZELM
RDRL WMP
S SCHOENFELD
RDRL WMP B
S SATAPATHY
A SOKOLOW
T WEERASOORIYA
RDRL WMP C
R BECKER
S BILYK
T BJERKE
D CASEM
J CLAYTON
D DANDEKAR
M GREENFIELD
B LEAVY
J LLOYD
S SEGLETES
A TONGE
C WILLIAMS
RDRL WMP D
R DONEY
C RANDOW

INTENTIONALLY LEFT BLANK.